Supplementary Information

Autofluorescence spectroscopy for quantitative analysis of cellulose nanocrystals

Marcus A. Johns,[*] Jude Abu-Namous, Hongying Zhao, Michael Gattrell, James Lockhart, Emily D. Cranston

Table of Contents

1. Results and Discussion
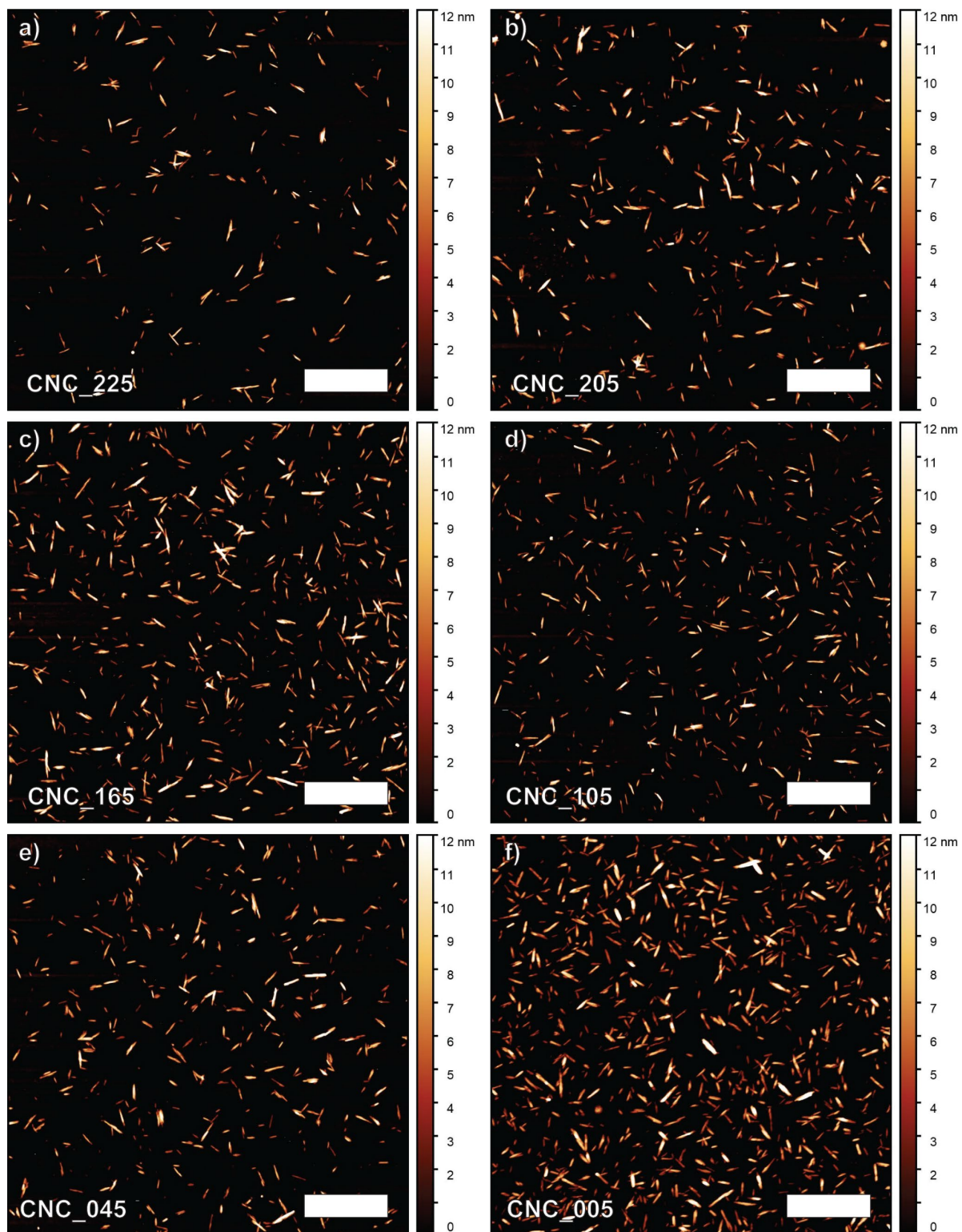
1.1 AFM analysis of lab-made CNCs

Figure S1. Representative AFM height images for a) CNC_225, b) CNC_205, c) CNC_165, d) CNC_105, e) CNC_045, f) CNC_005. Scale bars: 1 μm.
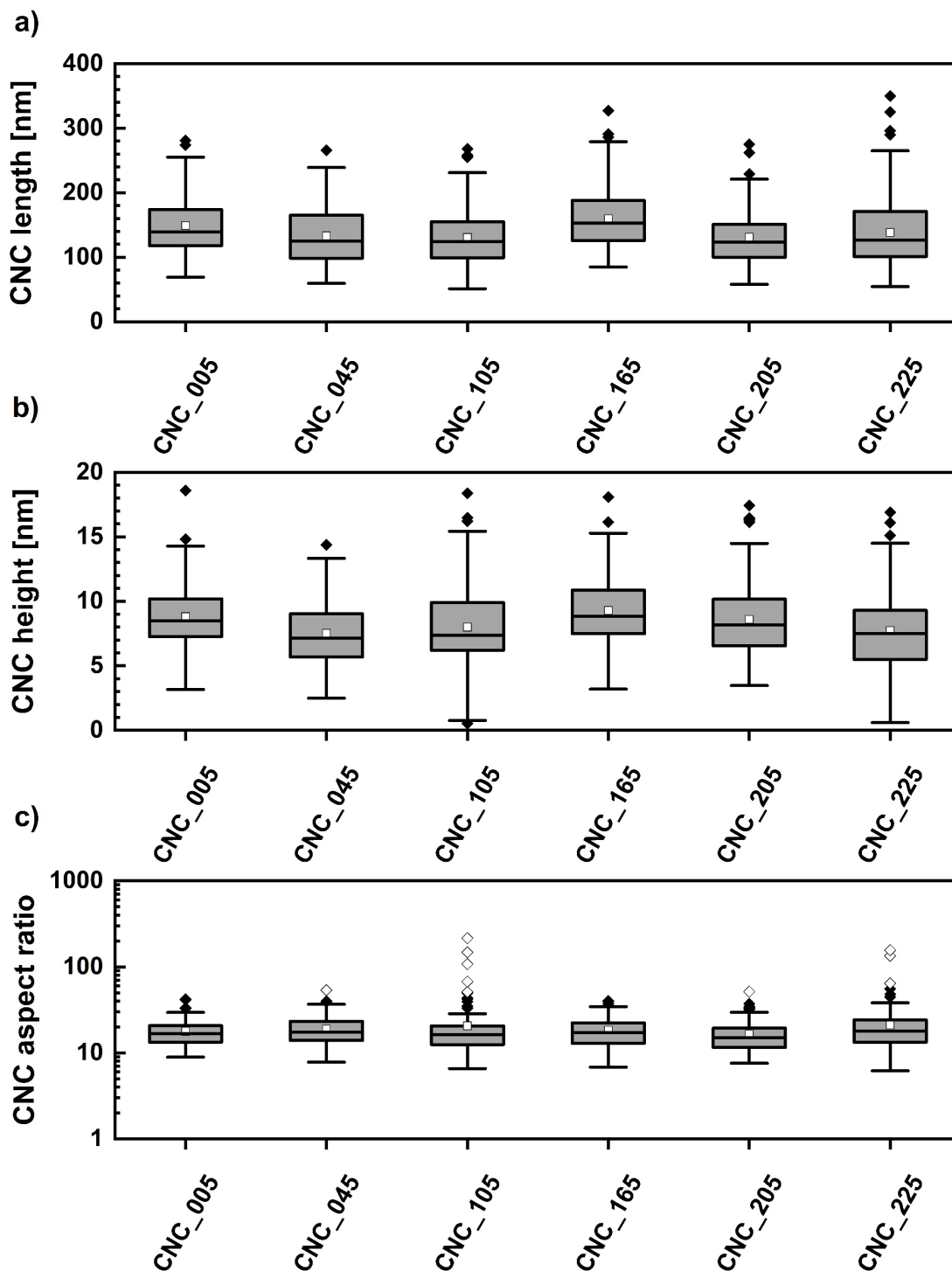
Figure S2. Distribution of desulfated CNC a) lengths, b) heights, and c) aspect ratios, determined by atomic force microscopy, as a function of degree of desulfation. White, filled squares: mean value; black, filled diamonds: outliers; black, open diamonds: extreme outliers. Top and bottom of bars represent the largest and smallest values measured excluding outliers, defined as either being greater than the 3rd quartile minus 1.5 times the interquartile range, or smaller than the 1st quartile minus 1.5 times the interquartile range respectively (n = 150).

1.2 Liquid crystalline self-assembly analysis of lab-made CNCs

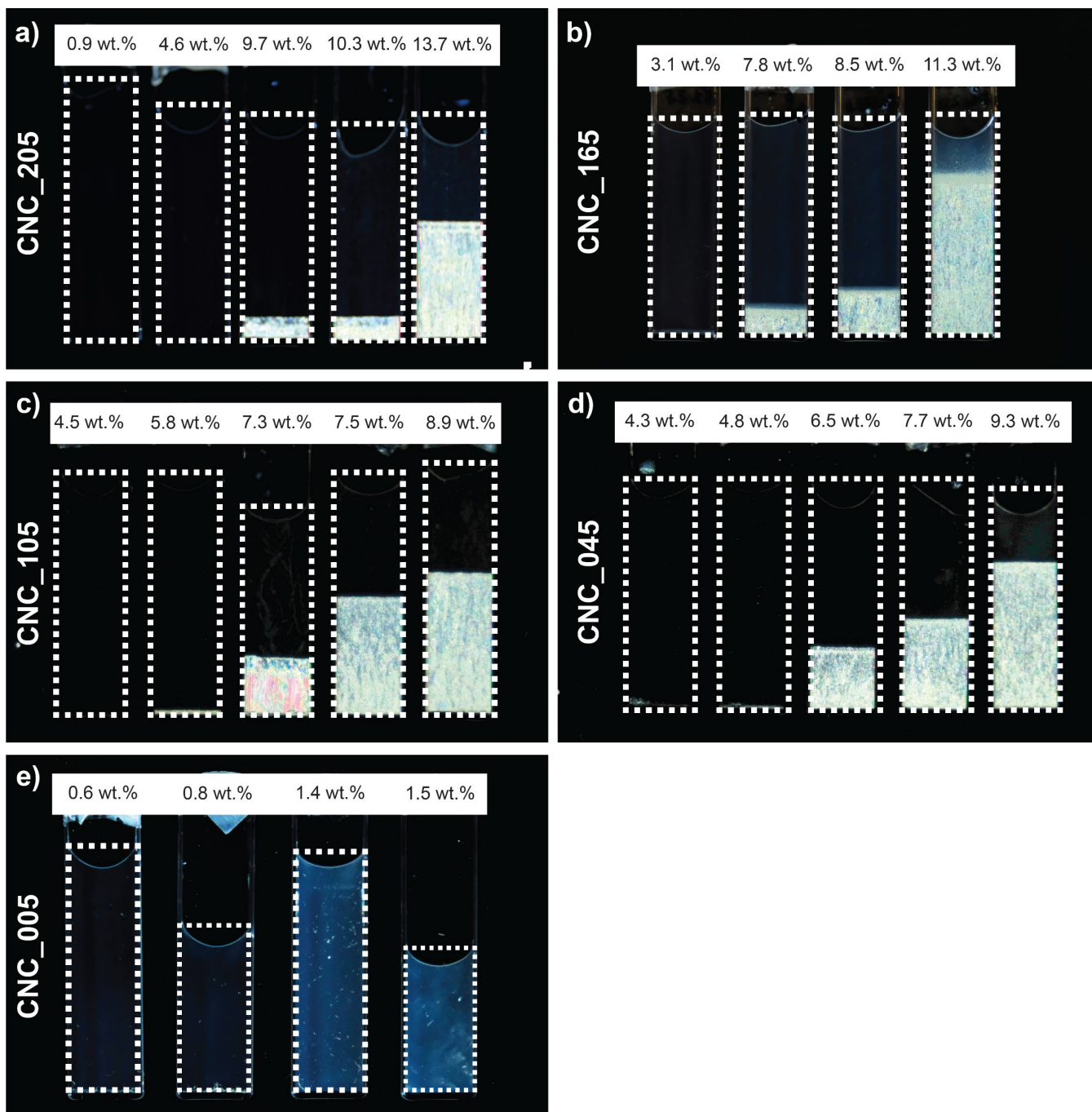Figure S3. Isotropic/anisotropic phase separation of a) CNC_205, b) CNC_165, c) CNC_105, d) CNC_045 samples in capillary tubes between crossed-polarizers; e) CNC_005 did not exhibit phase separation but gelation could be observed at higher concentrations under polarized light. White dashed lines outline the suspension volume in the capillaries and bright streaky areas correspond to the anisotropic (chiral nematic) phase.
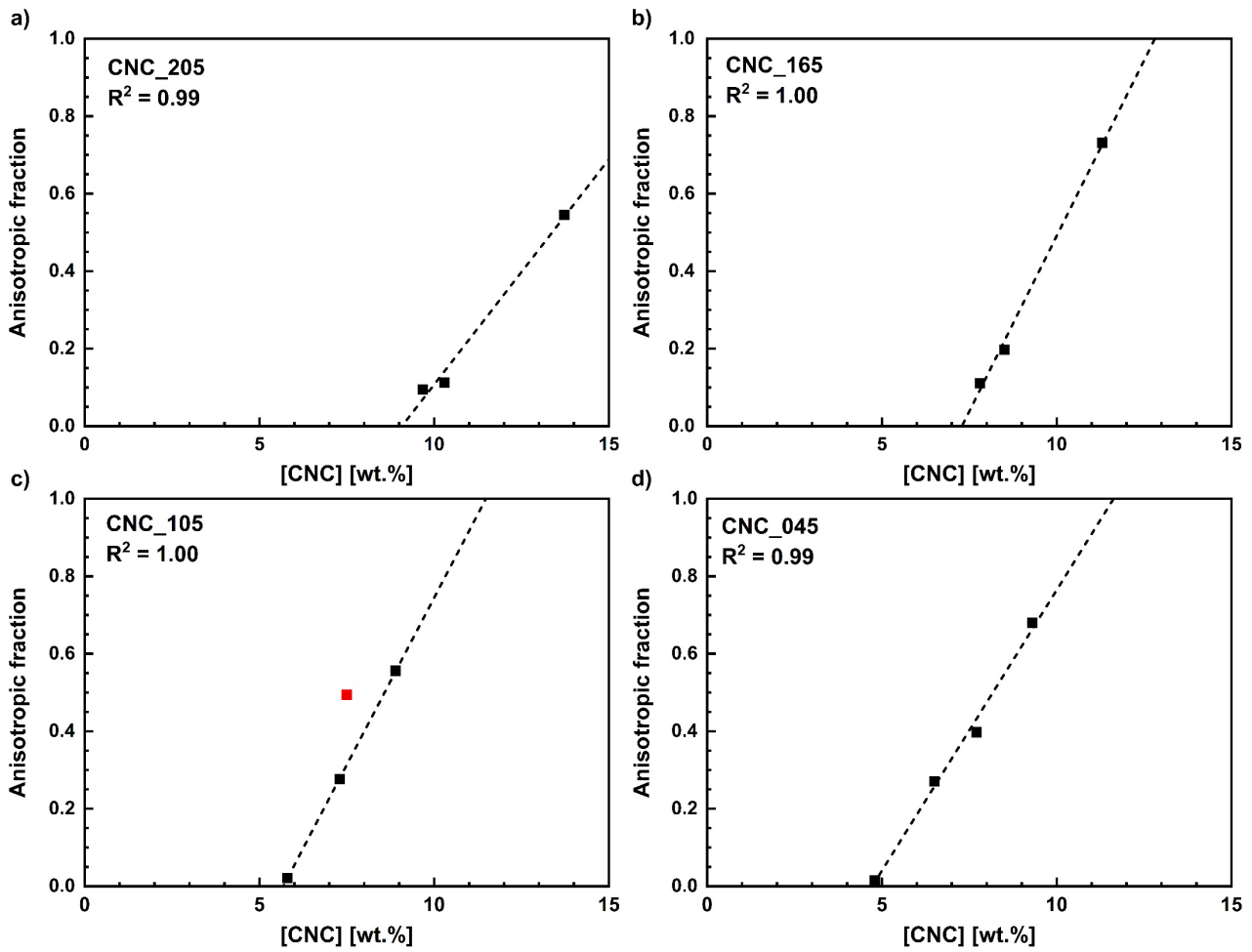
Figure S4. Effect of CNC concentration on anisotropic:isotropic phase separation ratio, used to determine c^* for a) CNC_205, b) CNC_165, c) CNC_105, and d) CNC_045 (black, dashed line: linear line of best fit; red square: outlier determined by Q test on residual errors).

1.3 Fluorescent intensity curves

Figure S5. Dependence of total intensity of the fluorescent spectrum on CNC concentration for a range of commercial and lab-made CNCs in suspension: a) Celluforce, b) NORAM (as-received), c) NORAM (dialyzed), d) CNC_225, e) CNC_205, f) CNC_165, g) CNC_105, h) CNC_045, and i) CNC_005 (black, dashed line: linear line of best fit; error bars: ±SE for N = 3, n = 5).

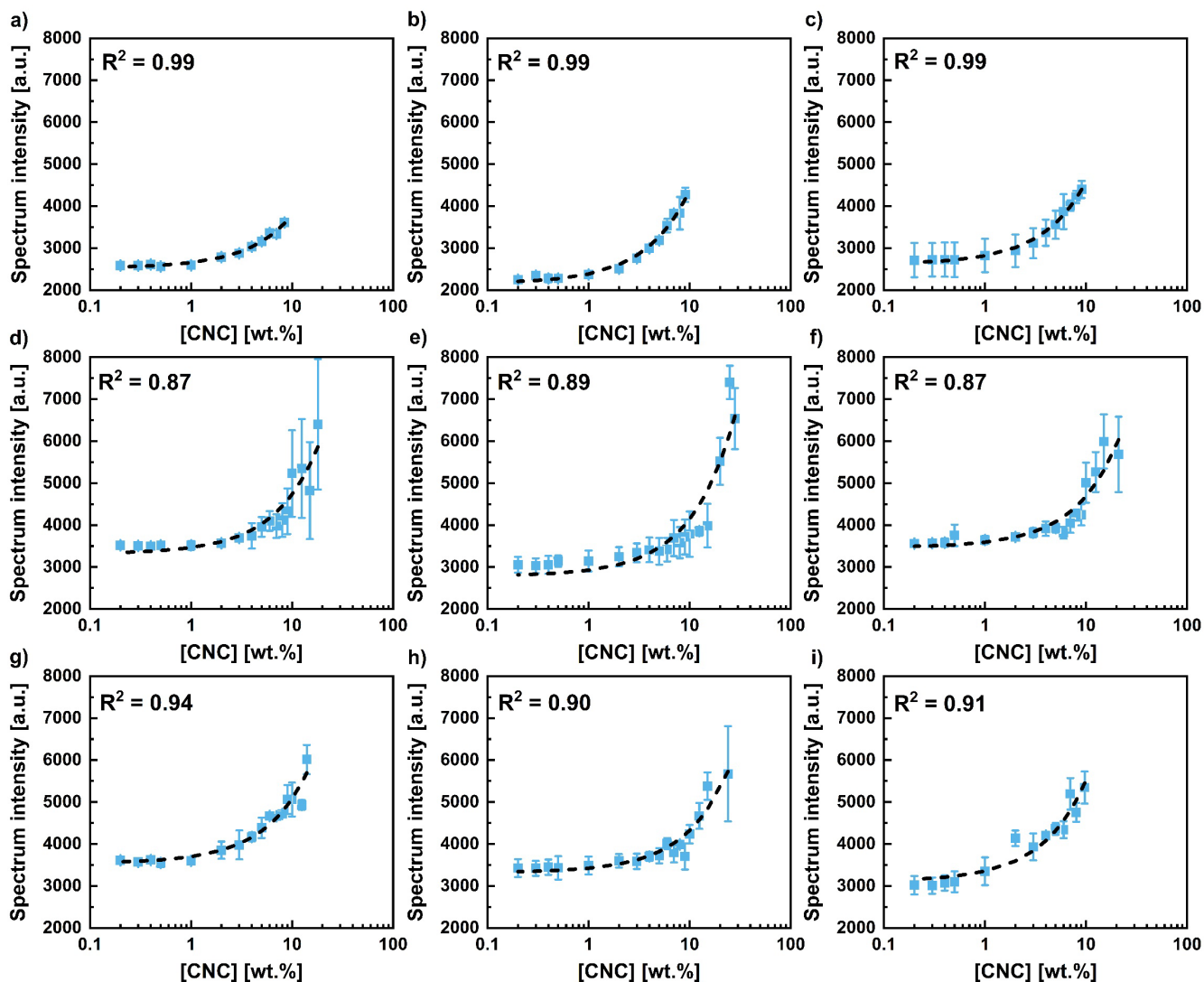**1.4 Consideration of Raman band from surface bound water**

Hydrogen bonding arising from water bound to the particle surface has a characteristic peak between 3450-3300 cm^{-1},[1] which corresponds to an emission wavelength of 470-467 nm under excitation at 405 nm. To confirm that the 470 nm band we assigned to fluorescence arising from hydrogen bonding between cellulose chains was not confounded with the Raman band, or that the emission was purely due to the Raman band and the fluorescent band was not real, additional experiments were performed on Celluforce CNCs in both the wet and dry states. Acquisition of the fluorescent spectrum for CNC suspensions via an FLS1000 spectrometer (Edinburgh Instruments, Livingston, UK) revealed the presence of the Raman band, which dominated the spectrum at low concentrations (Figure S6a).
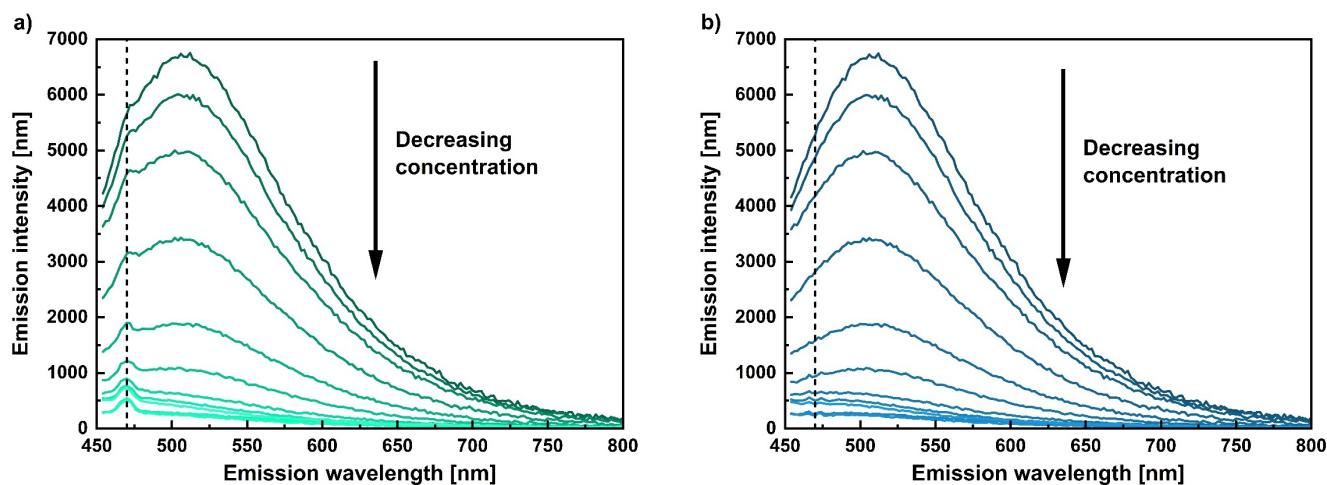

Figure S6. a) Detection of Raman band associated with surface bound water in fluorescent spectra acquired from spectrometer. b) Fluorescent spectra after removal of Raman band (CNC suspension concentration range: 7.0 – 0.2 wt.%; black dashed line: λ = 470 nm).

After removal of the Raman band via deconvolution of the spectra (Figure S6b), the average fluorescent band maximum is observed to be at 505 nm above 1 wt.%, shifting to 468 nm below 1 wt.%. This suggests that the fluorescent spectra consist of at least two independent bands centred at these wavelengths, which agrees with the confocal spectroscopy data used to determine the CNC properties. Furthermore, confocal analysis of the Celluforce CNCs in the dry state still showed the characteristic shoulder at 470 nm, whilst no Raman band was observed in the spectrum acquired using the spectrometer (Figure S7). This provides further evidence that the shoulder observed in the confocal data is not due to the Raman band.
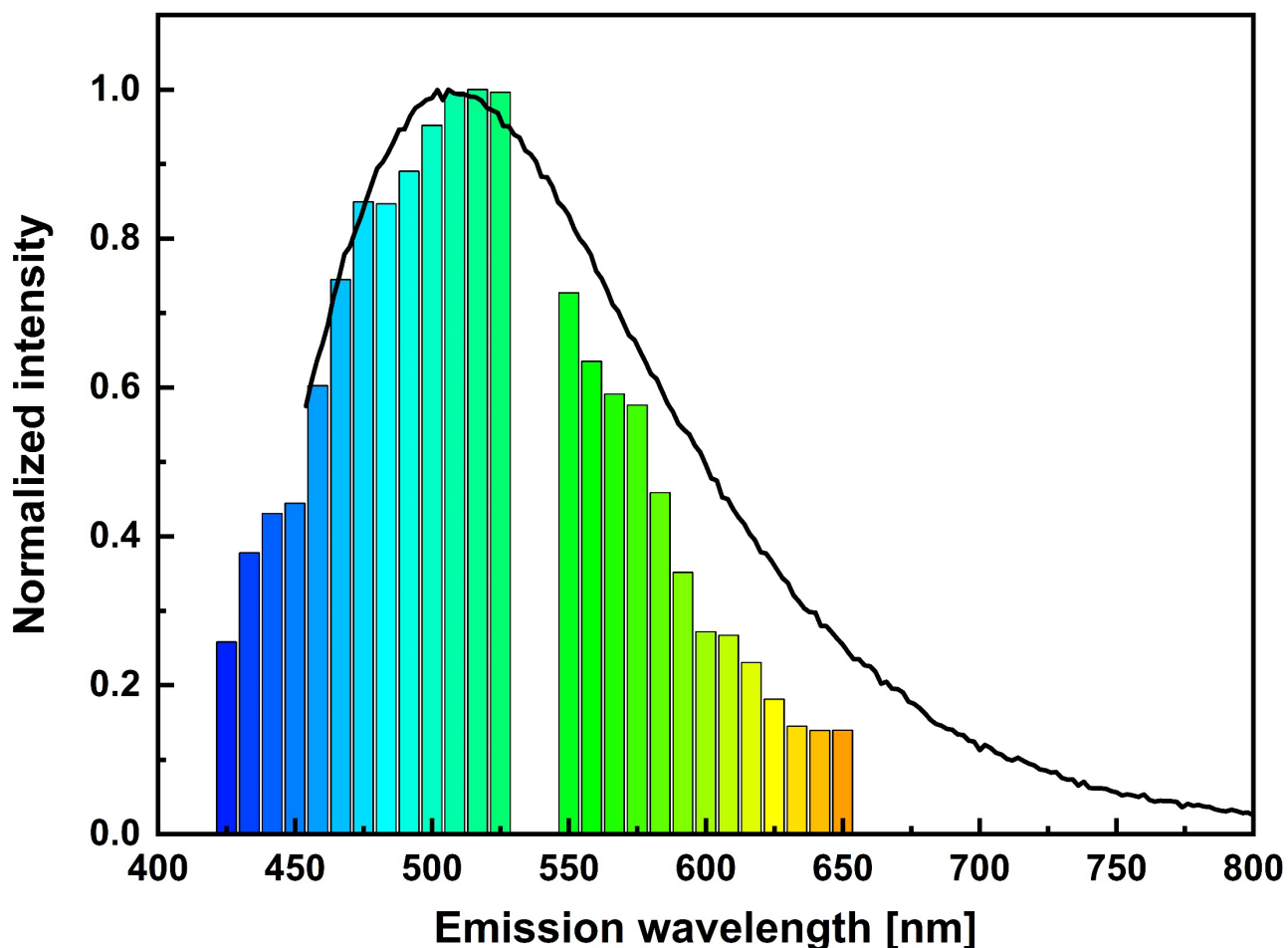
Figure S7. Overlay of fluorescent spectra for dry Celluforce CNCs acquired via confocal spectroscopy (coloured bars) and via a spectrometer (black solid line). Whilst the shoulder at 470 nm is present in the confocal spectrum, no Raman band associated with surface bound water is observed in the spectrometer spectrum.

The c^* for Celluforce CNCs was determined to be 1.3 ± 0.0 wt.% via the spectrometer data without removal of the Raman band (Figure S8a), which was significantly different ($p < 0.05$) to that determined via the confocal technique (3.4 ± 0.4 wt.%). In contrast, c^* was calculated to be 2.7 ± 0.4 wt.% after removal of the Raman band (Figure S8b), which was not significantly different to the confocal analysis. Additionally, the initial 470:505 nm ratio after the band removal was similar to that determined via confocal analysis, which was not the case with the Raman band present (value more than doubled).
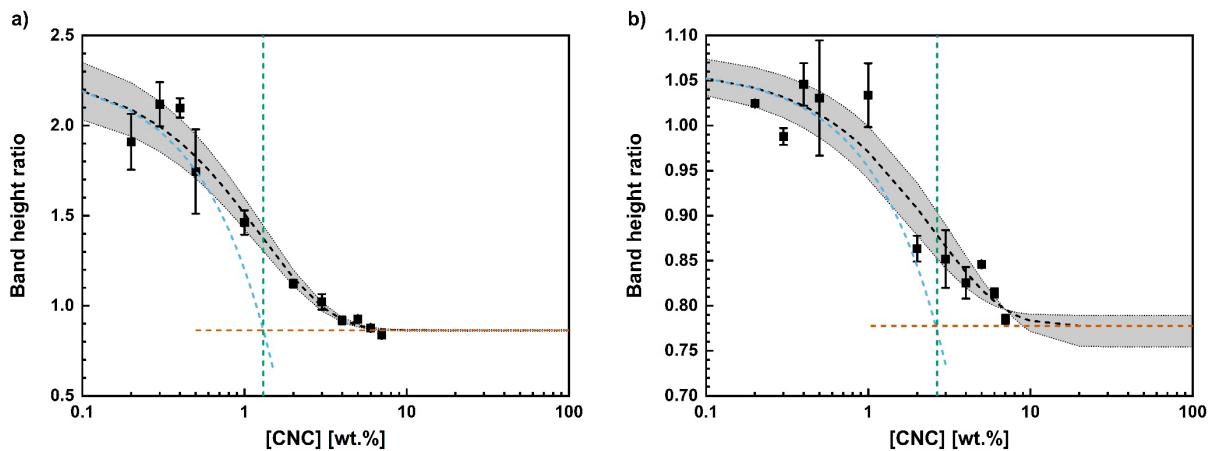
Figure S8. Determination of critical concentration via spectrometer for Celluforce CNCs a) without removal of the Raman band, b) with removal of the Raman band (black squares: data used to determine line of best fit; black dashed line: line of best fit, $y = Ae^{1-Bx} + C$; grey enclosed area: $y \pm SE = Ae^{1-Bx} + C$; blue dashed line: linear fit to initial gradient; orange line: linear fit to final gradient; green line: intersection of linear gradients. Error bars: $\pm$ SE for N = 2, n = 1).

Considering the evidence presented, we are confident that the Raman band is not present in the analysed confocal data. This is most likely due to differences in the optical set-up of the two instruments (e.g. beam splitter with charge-coupled device camera in the confocal microscope *vs* monochromator and photomultiplier tube in the spectrometer). We conclude that the band observed at 470 nm in the confocal data is due to autofluorescence alone.

1.5 Mathematical consideration of variation in intensity ratio with concentration

The intraparticle fluorescence intensity ($I_{\lambda=470}$) is independent of changes in the CNC physicochemical environment and, therefore, is directly proportional to the number of particles present, i.e., the CNC concentration ($[CNC]$), Equation S1:

$$I_{\lambda=470} \propto [CNC] \qquad (S1)$$

However, the total interparticle fluorescence intensity ($I_{\lambda=505}$) is dependent on the surface density of the heteroatom-containing chemical group that contributes to the fluorescence band (σ, mmol kg^{-1} CNC), the quantum efficiency of the fluorescence interaction involving the chemical group (Φ) and the total number of particle-particle interactions that result in fluorescence (n_i), Equation S2:

$$I_{\lambda=505} \propto \sigma \Phi n_i \qquad (S2)$$

Under dilute conditions (isotropic phase), assuming that the total number of particle-particle interactions is directly proportional to the number of interactions that result in fluorescence, an increase in concentration will not only increase the number of particles present but also the number of particle-particle interactions that each individual particle is involved in, resulting in a power dependence on the CNC concentration, Equation S3:

$$I_{\lambda=505,dilute} \propto \sigma \Phi [CNC]^2 \qquad (S3)$$

where $I_{\lambda=505,dilute}$ is the interparticle fluorescence intensity under dilute conditions. However, at the concentration at which the average particle will be interacting with the maximum number of other particles (formation of an anisotropic phase or gel), n_i will become linearly dependent on the CNC concentration, Equation S4:

$$I_{\lambda=505,network} \propto \sigma \Phi [CNC] \qquad (S4)$$

where $I_{\lambda=505,network}$ is the interparticle fluorescence intensity upon formation of a network.

Under dilute conditions, the 470:505 nm intensity ratio ($I_{\lambda=470}/I_{\lambda=505,dilute}$) will decrease with increasing concentration once the concentration is sufficient for the particles to begin to interact with one another, Equation S5:

$$I_{\lambda=470}/I_{\lambda=505,dilute} \propto [CNC]/[CNC]^2 = 1/[CNC] \qquad (S5)$$

Once the "network" is fully formed, i.e. every particle is interacting with a maximum number of other particles, the 470:505 nm intensity ratio ($I_{\lambda=470}/I_{\lambda=505,network}$) will become constant, Equation S6:

$$I_{\lambda=470}/I_{\lambda=505,network} \propto [CNC]/[CNC] = 1 \qquad (S6)$$

In the case of CNCs that form liquid crystalline phases, the concentrations that are considered dilute are those at which only the isotropic phase is observed, whilst the concentrations at which the network is considered fully formed are those at which only the anisotropic phase is observed. The transition ratio ($I_{\lambda=470}/I_{\lambda=505,transition}$) between these two regions, from c^* - at which the anisotropic phase is first observed - to the purely anisotropic phase will be dependent on the anisotropic fraction of the suspension (X), Equation S7:

$$I_{\lambda=470}/I_{\lambda=505,transition} \propto [CNC]/X[CNC] + (1-X)[CNC]^2 \qquad (S7)$$

Therefore, the 470:505 nm intensity ratio will initially decrease with increasing concentration before tending to a constant value above c^*.
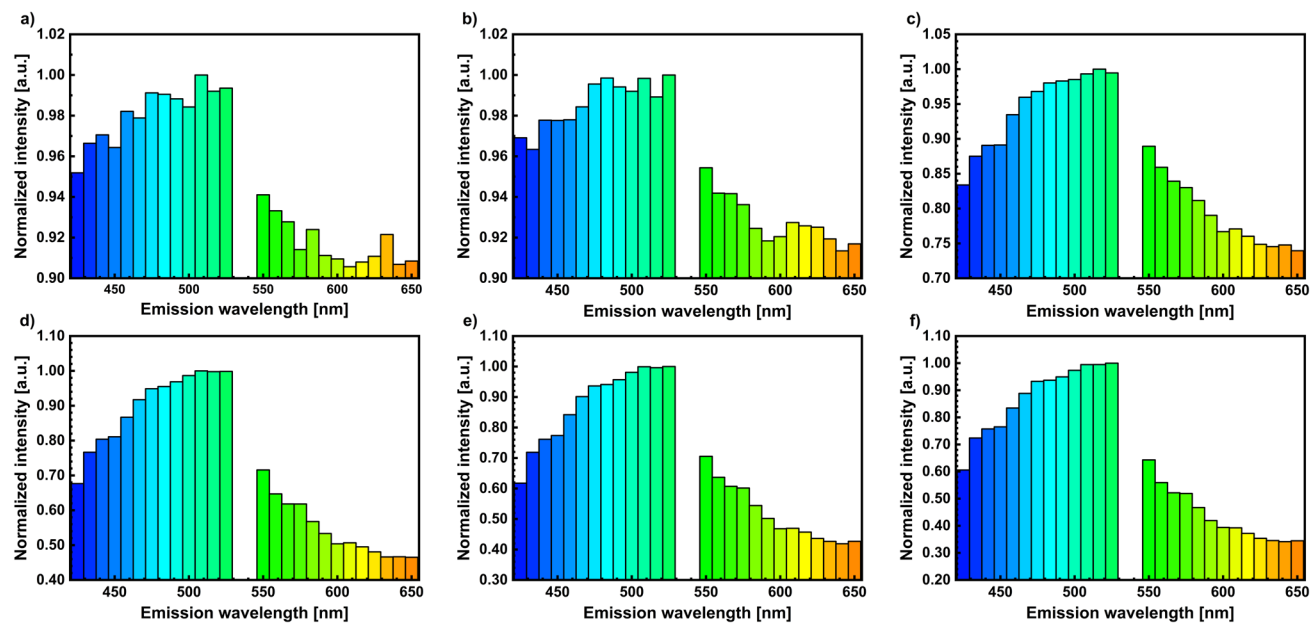
1.6 Determination of *c**/gel point curves

Figure S9. Average fluorescence spectrum of CNC_225 at a) 0.2 wt.%, b) 1.0 wt.%, c) 5.0 wt.%, d) 10.0 wt.%, e) 15.0 wt.%, and f) 18.0 wt.%. Spectra normalized to maximum value, note the change in the range of the y-axes with each sample.
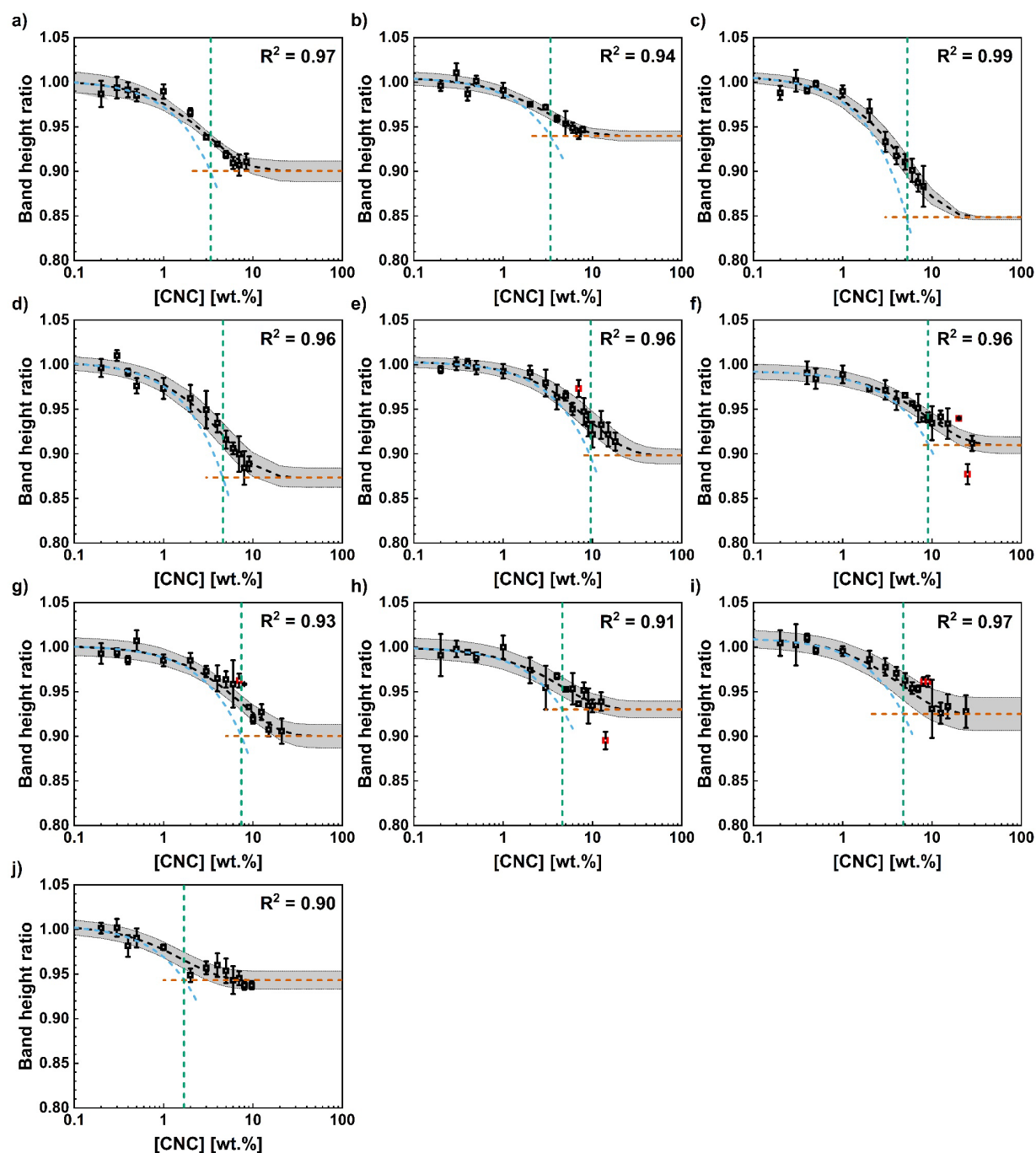
Figure S10. Determination of critical concentration via fluorescent spectroscopy technique for a) Celluforce CNCs, b) Anomera CNCs, c) NORAM CNCs (as-received), d) NORAM CNCs (dialyzed), e) CNC_225, f) CNC_205, g) CNC_165, h) CNC_105, i) CNC_045, j) CNC_005 (black open squares: data used to determine line of best fit; red open square: data treated as outliers as determined by Q test on residual errors; black dashed line: line of best fit, $y = Ae^{1-Bx} + C$; grey enclosed area: $y \pm SE = Ae^{1-Bx} + C$; blue dashed line: linear fit to initial gradient; orange line: linear fit to final gradient; green line: intersection of linear gradients. Error bars: $\pm$ SE for N = 3, n = 5).

1.7 Correlation of c^* curve constants with CNC properties

We considered whether the constants A, B, and C in Equation 1 determined for sulfated CNCs could be linked to their physicochemical properties. We determined that the surface charge content (σ, mmol kg^{-1} CNC) divided by the average CNC cylindrical volume ($V = \pi(h/2)^2 l$, nm^3) accounted for 79 and 82% of the variation for constants A and C, respectively (Figure S7a and Figure S7b) determined using Equations S8 and S9:

$$A = 0.40\left(\sigma/V\right) + 0.02 \tag{S8}$$

$$C = -1.06\left(\sigma/V\right) + 0.94 \tag{S9}$$

where h is the average cross-sectional height of the CNC sample (nm) and l is the average length of the CNC sample (nm) from AFM images. From a theoretical standpoint, these correlations are justified as constants A and C are dependent on the ratio of interparticle to intraparticle interactions that result in fluorescence for a single CNC. The surface charge content is equivalent to the number of interparticle interactions, whilst the volume of the CNC particle is an estimate of the number of intraparticle interactions, assuming that the CNC particle density is constant between samples. For constant B, the surface charge content divided by the CNC aspect ratio accounted for 67% of the variation (Figure S7c), increasing to 90% if the result for CNC_045 was considered an outlier (Figure S7d) determined using Equation S10:

$$B = -0.14\left(ln\left(\sigma\,{}^h/_l\right)\right) + 0.49 \tag{S10}$$

Considering that B defines c^* within Equation 1, the determined relationship agrees with the Onsager theory of the isotropic–nematic liquid crystal transition.[2] Onsager determined that an increase in the aspect ratio of a rod-like particle results in a decrease in c^*, whilst an increase in the electrostatic repulsion, approximated here by the surface charge content, effectively increases the diameter of the particle, leading to an increase in c^*.[2] Separate models would need to be developed for CNCs with different surface groups as these will affect the interparticle fluorescent quantum efficiency, changing the equations that predict constants A and C. We note that the equations for the three constants can be solved simultaneously, enabling approximate values for the average height and length of the CNCs to be determined from the fitted c^* curves if σ is known, although we did not test this here.
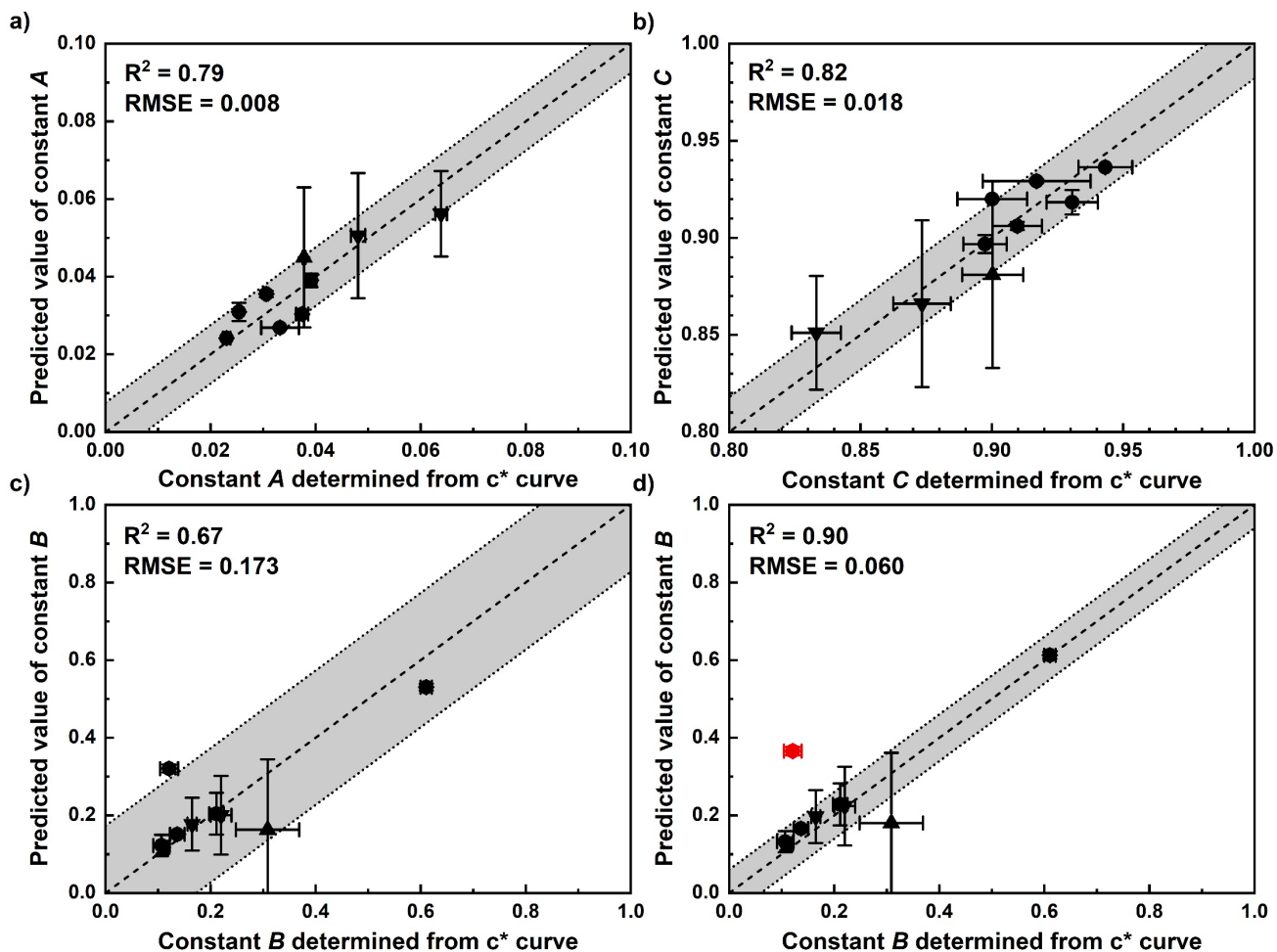
Figure S11. Values of constants for Equation 1 for sulfated CNCs as determined from c^* curves (Figure S10) vs. predicted from CNC physicochemical parameters. a) Values for constant A, equation for predicted values: $A = 0.40(\sigma/V) + 0.02$ where σ is the CNC surface charge content (mmol kg^{-1} CNC), h is the average height of the CNCs (nm) and l is the average length of the CNCs (nm) from AFM measurements; b) Values for constant C, equation for predicted values: $C = -1.06(\sigma/V) + 0.94$; c) Values for constant B assuming no outliers, equation for predicted values: $B = -0.12\big(ln(\sigma\,h/l)\big) + 0.42$; d) Values for constant B assuming that the value for CNC_045 is an outlier, equation for predicted values: $B = -0.14\big(ln(\sigma\,h/l)\big) + 0.49$. For all four panels, physicochemical parameters determined in this work (circles) and obtained from Reid et al.[3] (triangle) and Delepierre et al.[4] (inverted triangles) (red: outlier; dashed line equation: $y = x$; dotted line equations: $y = x \pm RMSE$. Error bars: ± SD).

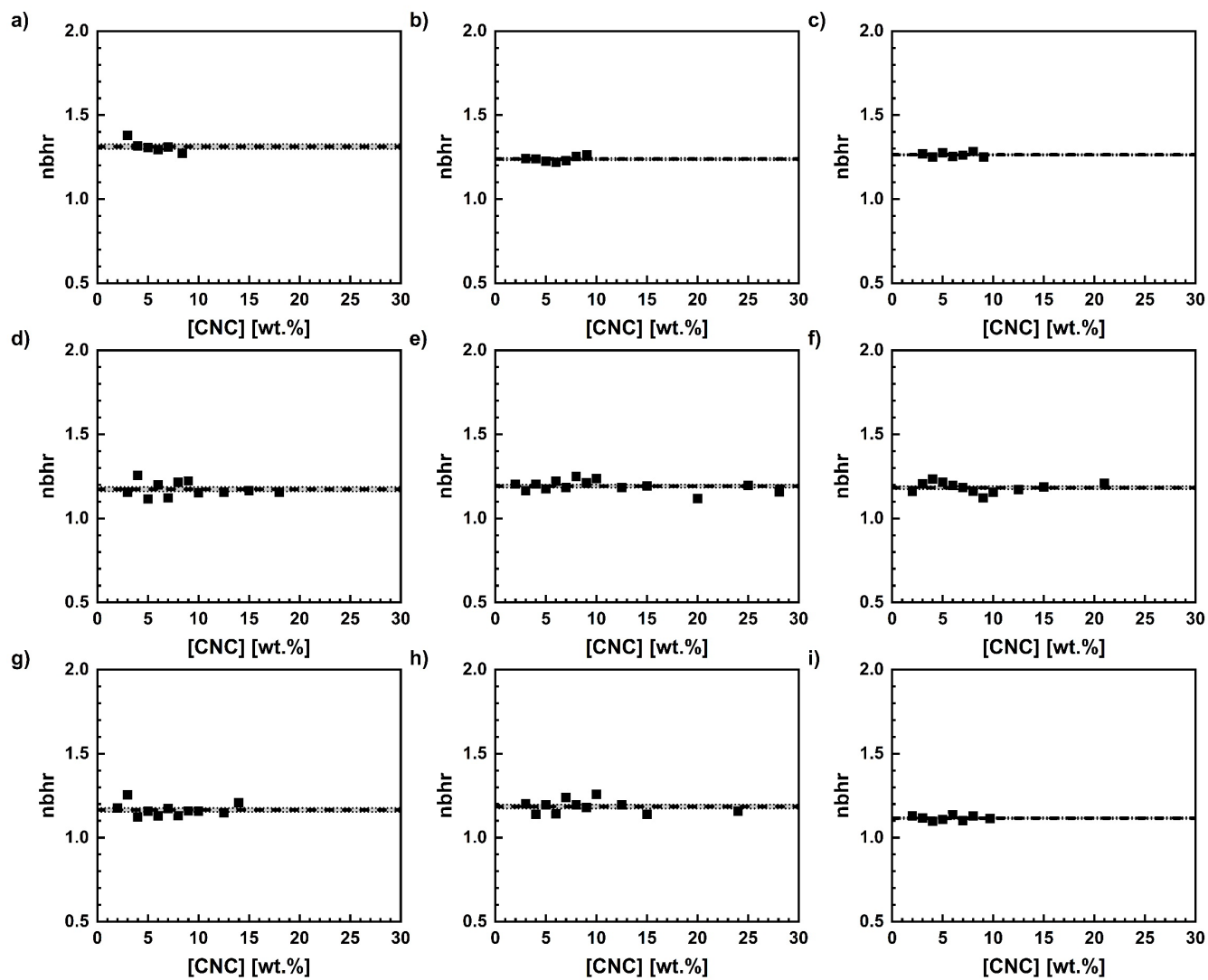## 1.8 Determination of σ from autofluorescence spectra

Figure S12. Fluorescent intensity ratio for 505:470 nm after normalization (nbhr) for a) Celluforce CNCs, b) NORAM CNCs (as-received), c) NORAM CNCs (dialyzed), d) CNC_225, e) CNC_205, f) CNC_165, g) CNC_105, h) CNC_045, i) CNC_005 (black dashed line: mean value; grey enclosed area: mean ± SE).
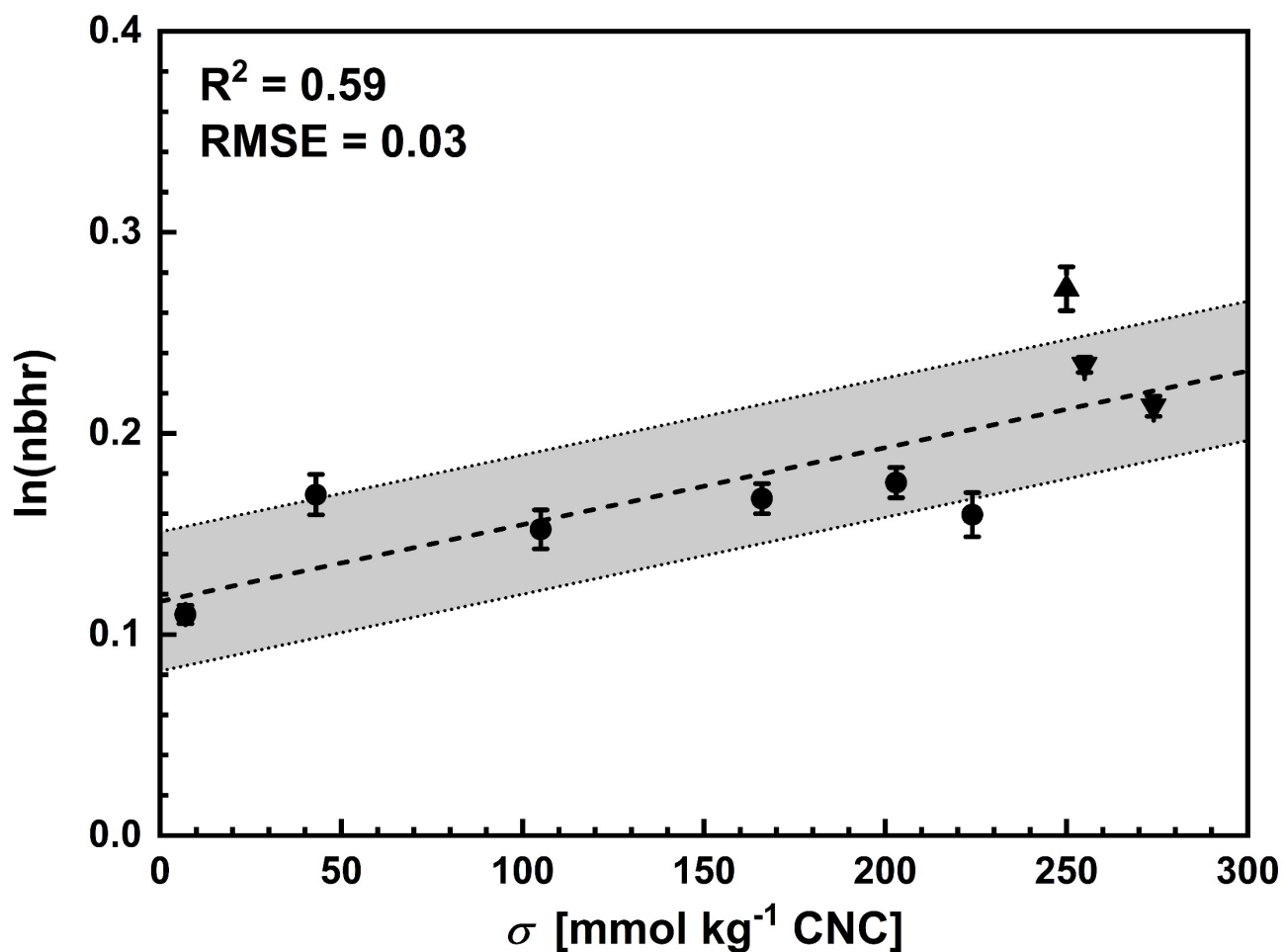
Figure S13. Correlation between natural log of the normalised band height ratio (ln(nbhr)) and σ of sulfated CNCs as determined by conductometric titration. The σ values were determined in this work (circles) and obtained from Reid et al.[3] (triangle) and Delepierre et al.[4] (inverted triangles) (dashed line equation: $y = mx + c$; dotted line equations: $y = mx + c \pm RMSE$. Error bars: $\pm$ SE for N = 9, n $\geq$ 5). This weak correlation with normalised data was remedied through Gaussian fitting of the normalised spectra as discussed in the main text.
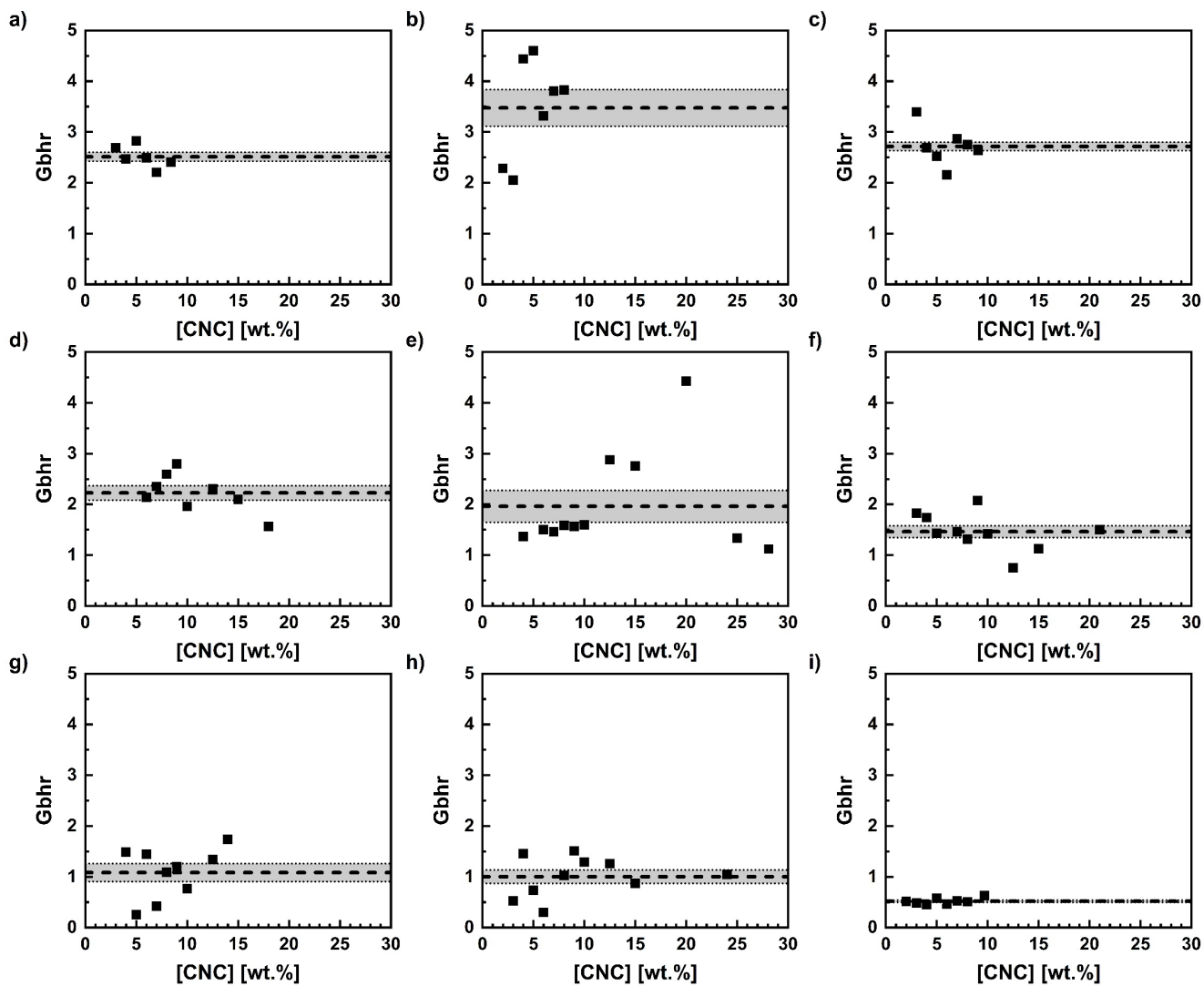
Figure S14. Deconvoluted Gaussian band height ratio (Gbhr) for a) Celluforce CNCs, b) NORAM CNCs (as-received), c) NORAM CNCs (dialyzed), d) CNC_225, e) CNC_205, f) CNC_165, g) CNC_105, h) CNC_045, i) CNC_005 (Black dashed line: mean value; grey enclosed area: mean ± SE).

2. References

[1] G. Socrates, *Infrared and Raman Characteristic Group Frequencies: Tables and Charts*, John Wiley & Sons, Ltd, **2004**.

[2] L. Onsager, *Ann. N. Y. Acad. Sci.* **1949**, *51*, 627–659.

[3] M. S. Reid, M. Villalobos, E. D. Cranston, *Langmuir* **2017**, *33*, 1583–1598.

[4] G. Delepierre, O. M. Vanderfleet, E. Niinivaara, B. Zakani, E. D. Cranston, *Langmuir* **2021**, *37*, 8393–8409.